Eur. Phys. J. C 29, 103–109 (2003)
Digital Object Identifier (DOI) 10.1140/epjc/s2003-01206-5

THE EUROPEAN PHYSICAL JOURNAL C

Model-independent constraints on contact interactions from LEP2 data analysis

A.A. Babich[1,2], G. Della Ricca[3], J. Holt[4], P. Osland[5], A.A. Pankov[1,3], N. Paver[3]

[1] Pavel Sukhoi Technical University, Gomel 246746, Belarus
[2] ICTP, 34014 Trieste, Italy
[3] University of Trieste and INFN-Sezione di Trieste, 34100 Trieste, Italy
[4] CERN, 1211 Geneva 23, Switzerland
[5] Department of Physics, University of Bergen, Allégaten 55, 5007 Bergen, Norway

Received: 18 December 2002 / Revised version: 19 March 2003 /
Published online: 13 May 2003 – © Springer-Verlag / Società Italiana di Fisica 2003

Abstract. We derive model-independent constraints on four-fermion contact interaction-type dynamics from the published preliminary LEP2 experimental data on e^+e^- annihilation into $\mu^+\mu^-$ and $\tau^+\tau^-$ pairs, measured at different energies between 130 and 207 GeV. The basic observables are chosen to be the total cross section and the forward–backward asymmetry, and the analysis realistically takes into account data uncertainties and correlations among measurements at the various energies. The combination of data from different energy points plays an important role in the determination of regions allowed for the contact interaction coupling constants. In contrast to the more common one-parameter analyses, we only obtain constraints on pairs of parameters rather than limits on individual ones.

1 Introduction

Many standard model extensions envisage a dynamics acting at one (or more) large mass scales $\Lambda \gg M_W$, such that the relevant states exchanged among quarks and leptons, having a mass proportional to Λ, are so heavy that they could not be directly produced at accelerator energies. The most familiar case is represented by quark and lepton composite models [1,2], but there are numerous other examples. However, such new interactions could manifest themselves by indirect, virtual, effects represented by deviations of the measured observables from the standard model (SM) predictions. If some deviations were effectively observed experimentally to a given significance level, one could try to derive from the data numerical information on the parameters (masses and coupling constants) of the non-standard models and, eventually, to select the viable one. In the case where, instead, no deviation from the SM predictions were observed within the experimental accuracy, one can set numerical bounds and/or constraints on the parameters characterizing the new interactions and, in particular, on the relevant mass scales Λ. This information should also be of phenomenological interest, in the exploration of non-standard interactions.

In the spirit of "effective" theories, exchanges of very heavy objects in reactions of quarks and leptons can be parameterized by a *contact interaction*, representing the "low energy" expansion of the transition amplitude to leading order in the small ratio $\sqrt{s}/\Lambda$ ($\sqrt{s}$ being the c.m. energy). The explicit form of such contact interaction Lagrangian (CI) depends on the particles participating in the reaction under consideration. Specifically, we consider here the electron–positron annihilation:

$$e^+ + e^- \to f + \bar{f}, \tag{1}$$

with $f = \mu$ and τ, and the relevant precision data at LEP2 for $130 < \sqrt{s} < 207\,\mathrm{GeV}$, published in [3], where the results of the four experimental collaborations are combined. Such high precision data can be regarded as a powerful tool to severely test manifestations of non-standard interactions through deviations from the SM predictions. In particular, we are interested in deriving, from those data, constraints on the *e e f f contact interaction* Lagrangian [2]:

$$\mathcal{L} = \sum_{\alpha\beta} g^2_{\mathrm{eff}}\, \epsilon_{\alpha\beta}\, (\bar{e}_\alpha \gamma_\mu e_\alpha)\left(\bar{f}_\beta \gamma^\mu f_\beta\right), \tag{2}$$

where $\alpha, \beta = \mathrm{L}, \mathrm{R}$ denote left- or right-handed fermion helicities, and the parameters $\epsilon_{\alpha\beta}$ specify the chiral structure of individual interactions and determine the size of the deviations from the SM predictions. One can introduce the previously mentioned large mass scales by $|\epsilon_{\alpha\beta}| = 1/\Lambda^2_{\alpha\beta}$, and conventionally fixing $g^2_{\mathrm{eff}}/4\pi = 1$ as a reminder that, as a compositeness remnant force, this interaction would become strong at $\sqrt{s} \sim \Lambda_{\alpha\beta}$. However, as remarked above, more generally the scales $\Lambda_{\alpha\beta}$ define a standard to compare the sensitivity of measurements to the various kinds of new interactions; see, e.g., [4,5].

In practice, the situation is complicated by the fact that, for a given fermion flavor f, (2) defines four individual and independent models (basically, the combinations of the four chiralities α, β through the ϵ) and, in principle, the general contact interaction could be any linear combination of these models. Thus, the aforementioned deviations of the cross section from the SM predictions may simultaneously depend on *all* four-fermion effective couplings and, if only one value of the c.m. energy were available, the straightforward comparison of deviations and experimental uncertainty could produce only numerical correlations among the different CI couplings, rather than separate, and restricted, allowed regions for these parameters in the parameter space around the SM limit $\epsilon_{\alpha\beta} = 0$. Moreover, negative interference of CI and SM amplitudes in the cross section might considerably weaken the bounds.

The simplest and commonly adopted procedure consists in assuming non-zero values for just one of the $\epsilon_{\alpha\beta}$ at a time, and in constraining it to a finite interval by essentially a χ^2 fit analysis of the measured cross sections and forward–backward asymmetries, while all the other parameters are set equal to zero [4–6]. In this way, only tests of specific models can be performed.

On the other hand, it would be desirable to perform a more general kind of analysis of the data, that simultaneously includes all terms of (2) as free, potentially non-vanishing independent parameters and, at the same time, allows one to disentangle their contributions to the basic observables in order to derive separate constraints within finite regions around the SM limit.

In cases where only one value for the c.m. energy is available, such as for the planned e^+e^- Linear Collider [7], a solution is represented by the initial electron beam's longitudinal polarization, that would enable to experimentally extract the individual helicity amplitudes of process (1), by definition directly related to the individual $e\ e\ f\ f$ contact couplings $\epsilon_{\alpha\beta}$ [8,9].

Such a procedure cannot be applied to the data from LEP, with unpolarized electron and positron beams. However, in this case, the cross sections of processes (1) are measured at LEP2 over a range of $\sqrt{s}$ values wide enough that the energy dependence of the deviations, entirely determined by well-known SM parameters, can be exploited to restrict the bounds to limited regions in the CI parameter space, and in this way to perform an analysis of the new interaction, model-independent in the sense indicated above. This observation was used for a global analysis of data at the energies of LEP1, LEP2 and TRISTAN in [10]. The analysis presented here uses exclusively the most recent higher statistics LEP2 data, combines the two channels $\mu^+\mu^-$ and $\tau^+\tau^-$ and the results of the four experiments, and accounts for, among other things, the correlations among the measurements at the different energy points. The basic observables will be the "conventional" ones, namely, the integrated cross section $\sigma(s)$ and the forward–backward asymmetry $A_{\rm FB}(s)$, whose experimental values are tabulated in [3].

Specifically, in Sect. 2 we will give the basic definition of helicity amplitudes and the formulae relevant to σ and $A_{\rm FB}$ for the processes of interest here, and in Sect. 3 we shall present the model-independent analysis of LEP2 data and the resulting constraints on CI couplings. Finally, Sect. 4 will be devoted to some concluding remarks and an application of the method to a model example.

2 Cross section and helicity amplitudes

Limiting ourselves to the cases $f = \mu, \tau$ and neglecting all fermion masses with respect to $\sqrt{s}$, and taking into account the Born γ- and Z-exchanges in the s-channel plus the *contact interaction* term (2), the differential cross section of process (1) reads [11]

$$\frac{\mathrm{d}\sigma}{\mathrm{d}\cos\theta} = \frac{3}{8}\left[(1+\cos\theta)^2\sigma_+ + (1-\cos\theta)^2\sigma_-\right], \qquad (3)$$

where θ is the angle between the incoming electron and the outgoing fermion in the c.m. frame. In terms of helicity cross sections, $\sigma_{\alpha\beta}$ with $\alpha, \beta = \mathrm{L}, \mathrm{R}$:

$$\sigma_+ = \frac{1}{4}\left(\sigma_{\rm LL} + \sigma_{\rm RR}\right), \qquad (4)$$

$$\sigma_- = \frac{1}{4}\left(\sigma_{\rm LR} + \sigma_{\rm RL}\right). \qquad (5)$$

In (4) and (5)

$$\sigma_{\alpha\beta} = \sigma_{\rm pt}|\mathcal{M}_{\alpha\beta}|^2, \qquad (6)$$

where $\sigma_{\rm pt} \equiv \sigma(e^+e^- \to \gamma^* \to l^+l^-) = 4\pi\alpha^2_{\rm e.m.}/3s$ (for quark–antiquark production a color factor $N_C \simeq 3(1 + \alpha_s/\pi)$ would be needed). The helicity amplitudes $\mathcal{M}_{\alpha\beta}$ can be written as

$$\mathcal{M}_{\alpha\beta} = Q_eQ_f + g^e_\alpha\, g^f_\beta\, \chi_Z + \frac{s}{\alpha_{\rm e.m.}}\epsilon_{\alpha\beta}, \qquad (7)$$

where $\chi_Z = s/(s - M_Z^2 + \mathrm{i}M_Z\Gamma_Z)$ is the Z propagator; $g^f_{\rm L} = (I^f_{3L} - Q_f s^2_{\rm W})/s_{\rm W}c_{\rm W}$ and $g^f_{\rm R} = -Q_f s^2_{\rm W}/s_{\rm W}c_{\rm W}$ are the SM left- and right-handed fermion couplings of the Z with $s^2_{\rm W} = 1 - c^2_{\rm W} \equiv \sin^2\theta_{\rm W}$; $Q_e = Q_f = -1$ are the fermion electric charges.

The measured observables σ and $A_{\rm FB}$ are given by the relations:

$$\sigma = \int_{-1}^{1}\frac{\mathrm{d}\sigma}{\mathrm{d}\cos\theta}\,\mathrm{d}\cos\theta = \frac{1}{4}\left[(\sigma_{\rm LL} + \sigma_{\rm RR}) + (\sigma_{\rm LR} + \sigma_{\rm RL})\right], \qquad (8)$$

and

$$\sigma_{\rm FB} \equiv \sigma\, A_{\rm FB} = \left(\int_0^1 - \int_{-1}^0\right)\frac{\mathrm{d}\sigma}{\mathrm{d}\cos\theta}\,\mathrm{d}\cos\theta = \frac{3}{16}\left[(\sigma_{\rm LL} + \sigma_{\rm RR}) - (\sigma_{\rm LR} + \sigma_{\rm RL})\right]. \qquad (9)$$

Finally, their relation to $\sigma_\pm$ is given by

$$\sigma_\pm = \frac{\sigma}{2}\left(1 \pm \frac{4}{3}A_{\rm FB}\right). \qquad (10)$$

Table 1. Approximate average integrated luminosity per experiment and nominal center-of mass energies collected during LEP2 operations [3]

$E_{\rm CM}$ (GeV)	130	136	161	172	183	189	192	196	200	202	205	207
$\mathcal{L}_{\rm int}$ (pb^{-1})	3	3	10	10	50	170	30	80	80	40	80	140

Taking (7) into account, (8) and (9) show that σ and $\sigma_{\rm FB}$ (or $A_{\rm FB}$) simultaneously depend on *all* four contact interaction couplings, and therefore by themselves do not allow a model-independent analysis, but only the simplified one-parameter fit of individual models. However, σ and $\sigma_{\rm FB}$ depend on the two combinations of helicity cross sections $(\sigma_{\rm LL}+\sigma_{\rm RR})$ and $(\sigma_{\rm LR}+\sigma_{\rm RL})$. Accordingly, a combined analysis of σ and $\sigma_{\rm FB}$ enables to separately constrain the pairs of parameters $(\epsilon_{\rm LL},\epsilon_{\rm RR})$ and $(\epsilon_{\rm LR},\epsilon_{\rm RL})$. Moreover, the combination of experimental data on σ and $\sigma_{\rm FB}$ at different values of the c.m. energy allows to further restrict such separate bounds in a model-independent way.

To clarify this statement and intuitively show by a simplified example the role of the different energy points in improving the constraints, assuming that no deviation from the SM is observed within the experimental accuracies, constraints on the contact interaction couplings $\epsilon_{\alpha\beta}$ can be derived from the system of two inequalities:

$$|\sigma^{\rm SM+CI}-\sigma^{\rm SM}|<\delta\sigma, \tag{11}$$

$$|A_{\rm FB}^{\rm SM+CI}-A_{\rm FB}^{\rm SM}|<\delta A_{\rm FB}, \tag{12}$$

where $\delta\sigma$ and $\delta A_{\rm FB}$ represent the experimental uncertainties on these observables. Taking (4) and (5) into account, the deviations from the SM predictions in the left-hand sides of (11) and (12) can be written as

$$\sigma^{\rm SM+CI}-\sigma^{\rm SM}=\frac{1}{4}\Big[(\Delta\sigma_{\rm LL}+\Delta\sigma_{\rm RR}) + (\Delta\sigma_{\rm LR}+\Delta\sigma_{\rm RL})\Big], \tag{13}$$

$$A_{\rm FB}^{\rm SM+CI}-A_{\rm FB}^{\rm SM}=\frac{3}{16\,\sigma^{\rm SM}}\left[\left(1-\frac{4}{3}A_{\rm FB}^{\rm SM}\right)\times(\Delta\sigma_{\rm LL}+\Delta\sigma_{\rm RR}) - \left(1+\frac{4}{3}A_{\rm FB}^{\rm SM}\right)(\Delta\sigma_{\rm LR}+\Delta\sigma_{\rm RL})\right], \tag{14}$$

where $\Delta\sigma_{\alpha\beta}=\sigma_{\alpha\beta}^{\rm SM+CI}-\sigma_{\alpha\beta}^{\rm SM}$.

From (11)–(14) one can obtain constraints on the $\epsilon_{\alpha\beta}$. Specifically, the areas allowed to the values of the parameters are enclosed by concentric circles in the planes $(\epsilon_{\rm LL},\epsilon_{\rm RR})$ and $(\epsilon_{\rm LR},\epsilon_{\rm RL})$. For example, the domain allowed to the pair $(\epsilon_{\rm LL},\epsilon_{\rm RR})$ is delimited by the circular contours:

$$\left(\epsilon_{\rm LL}+\frac{\alpha_{\rm e.m.}}{s}\mathcal{M}_{\rm LL}^{\rm SM}\right)^2+\left(\epsilon_{\rm RR}+\frac{\alpha_{\rm e.m.}}{s}\mathcal{M}_{\rm RR}^{\rm SM}\right)^2=R_\pm^2, \tag{15}$$

where

$$R_\pm^2=\left(\frac{\alpha_{\rm e.m.}}{s}\mathcal{M}_{\rm LL}^{\rm SM}\right)^2+\left(\frac{\alpha_{\rm e.m.}}{s}\mathcal{M}_{\rm RR}^{\rm SM}\right)^2\pm\kappa^2, \tag{16}$$

and

$$\kappa^2=\left(\frac{\alpha_{\rm e.m.}}{s}\right)^2\frac{4}{\sigma_{\rm pt}}\delta\sigma_+. \tag{17}$$

In the right-hand side of (17), $\delta\sigma_+$ must be expressed in terms of the experimental uncertainties $\delta\sigma$ and $\delta A_{\rm FB}$ [1], and a color factor $1/N_C$ is needed in the case of quark–antiquark production. These relations show that both the center and the radii of the circles $R_\pm$ are determined by the values of the SM helicity amplitudes and depend on energy, while the width of the allowed area is determined by the experimental uncertainty of the observables. Therefore, in principle, the combination of two (or more) such allowed regions corresponding to different energies can lead to a reduction of the allowed region and, ultimately, to model-independent bounds on the contact interaction coupling constants.

It should be stressed that, while the observables are given by *two sums* of helicity cross sections, $\sigma_{\rm LL}+\sigma_{\rm RR}$ and $\sigma_{\rm LR}+\sigma_{\rm RL}$, it does *not* follow that one can only obtain constraints on the corresponding sums of parameters, $\epsilon_{\rm LL}+\epsilon_{\rm RR}$ and $\epsilon_{\rm LR}+\epsilon_{\rm RL}$. There is indeed a small, but finite, sensitivity to the individual parameters. This is due to effects proportional to squares of the ϵ parameters, together with the small difference between left- and right-handed couplings of the standard model, $|g_{\rm L}^\ell|\neq|g_{\rm R}^\ell|$.

3 Data fitting and derivation of constraints

Recently, the $f\bar{f}$ Subgroup of LEPEWWG presented preliminary combined results of measurements of the four LEP collaborations using experimental data from the full LEP2 available data set at energies from 130 GeV up to 207 GeV for the annihilation processes $e^+e^-\to f\bar{f}$ [3]. In particular, for lepton final states $f=\mu$ and τ, the set of the average cross sections $\sigma_{\mu\mu}$, $\sigma_{\tau\tau}$ and forward–backward asymmetries $A_{\rm FB}^{\mu\mu}$, $A_{\rm FB}^{\tau\tau}$ and their experimental errors have been given for the twelve energy points listed in Table 1.

The data fitting procedure used is based on the method of least squares. We introduce a χ^2 function, which may be written in the following matrix form:

$$\chi^2(\epsilon)=(\mathcal{O}^{\rm LEP2}-\mathcal{O}^{\rm TH}(\epsilon))^{\rm T}V^{-1}(\mathcal{O}^{\rm LEP2}-\mathcal{O}^{\rm TH}(\epsilon)), \tag{18}$$

where $\epsilon=(\epsilon_{\rm RR},\epsilon_{\rm LL},\epsilon_{\rm RL},\epsilon_{\rm LR})$ is the vector of CI parameters; $\mathcal{O}^{\rm LEP2}$ is the vector of values of observables measured at LEP2 and $\mathcal{O}^{\rm TH}$ is the vector of their theoretical predictions; finally, V is the covariance matrix of the experimental uncertainties.

[1] While σ_+ and σ_-, as shown in (4) and (5), are the most natural observables, we use instead σ and $A_{\rm FB}$ for our analysis, since the data are tabulated (with errors) for these observables

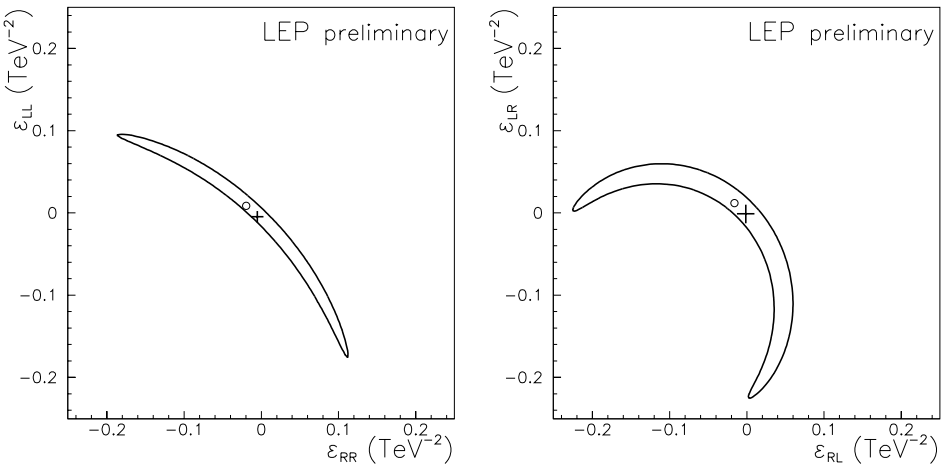

Fig. 1. Allowed areas at 95% C.L. on leptonic contact interaction parameters in the planes $(\epsilon_{\rm LL}, \epsilon_{\rm RR})$ and $(\epsilon_{\rm LR}, \epsilon_{\rm RL})$, obtained as projections of the four-dimensional confidence hypervolume on the relevant plane after minimization in the two remaining parameters. The bars correspond to one-dimensional model-dependent constraints as discussed in the text. The circles correspond to the central values (see Table 2)

The chosen set of observables, represented by the vector $\mathcal{O}^{\rm LEP2}$, contains 48 elements (two kinds of observable for two flavor channels and twelve energy points). The corresponding theoretical predictions, $\mathcal{O}^{\rm TH}$, which depend on the CI parameters ϵ and on radiative corrections via improved Born SM amplitudes [12,13], have been evaluated with $m_{\rm top} = 175\,{\rm GeV}$ and $m_H = 150\,{\rm GeV}$. Initial- and final-state radiation are taken into account by the program ZFITTER [14] adapted to the present case of contact interactions. The radiative corrections were applied using definition "2" in [3]: namely, for dilepton events $\sqrt{s'}$ is taken to be the bare invariant mass of the outgoing dilepton pair (as opposed to that of the s-channel propagator), the ISR-FSR photon interference is included and the signal is defined by the kinematical cut $\sqrt{s'} > 0.85\sqrt{s}$. We note that the improved Born amplitudes leave the form of the previous equations for the cross sections, (3) and (10) unaltered.

As regards the 48×48 symmetric covariance matrix V, the diagonal entries are the experimental uncertainties on the observables, while the off-diagonal entries define the correlations between the observables as well as among the different energy points [3].

The least-square confidence region is determined by the condition

$$\chi^2(\epsilon) \leq \chi^2_{\rm min} + \chi^2_{\rm CL}, \tag{19}$$

where $\chi^2_{\rm min}$ is the minimum value of the function $\chi^2(\epsilon)$ and $\chi^2_{\rm CL} = 9.49$ for 95% CL and four degrees of freedom. The procedure of minimization $\chi^2(\epsilon)$ is performed using the program package MINUIT [15].

Combining the μ and τ data, we show in Table 2 the components of the central value ϵ^0 (over-all minimum of χ^2) and the global limits (intervals $(\epsilon_{\rm min}, \epsilon_{\rm max})$) obtained as projections of the confidence region on the corresponding axes. These intervals should be considered as global, model-independent, constraints on the CI parameters $\epsilon_{\alpha\beta}$. The χ^2 in the model-independent fits amounted to 41.3, for $n_d = 48 - 4 = 44$ degrees of freedom: the probability of this result is $p = 0.411$ [16]. For comparison, we give the 95% CL one-parameter constraints on $\epsilon_{\alpha\beta}$ parameters for the LL, RR, LR and RL contact interaction models.

Table 2. Central value ϵ^0, global limits (allowed intervals) obtained as projections of the 95% CL four-dimensional region on the axes and 95% CL one-dimensional model-dependent constraints on the CI parameters

Parameter	Model independent		Model dependent
(TeV^{-2})	central value	global limits	
$\epsilon_{\rm LL}$	0.0085	$(-0.175, 0.095)$	$-0.0047^{+0.0071}_{-0.0071}$
$\epsilon_{\rm RR}$	-0.0195	$(-0.187, 0.111)$	$-0.0052^{+0.0078}_{-0.0078}$
$\epsilon_{\rm LR}$	0.0120	$(-0.225, 0.060)$	$-0.0012^{+0.0111}_{-0.0116}$
$\epsilon_{\rm RL}$	-0.0160	$(-0.225, 0.060)$	$-0.0012^{+0.0111}_{-0.0116}$

In Figs. 1 and 2 we show the contours which bound the regions found as "projections" of the four-dimensional confidence hypervolume determined by (19) on four of the two-dimensional planes (LL–RR), (LR–RL), (LL–LR), (LL–RL). The contours have been produced as the line connecting all points of the plane where χ^2 takes the value $\chi^2_{\rm min} + \chi^2_{\rm CL}$ after minimization on the two remaining free parameters.

These figures show obvious symmetries. First of all, in Fig. 1, where we display the allowed regions in the $(\epsilon_{\rm LL}, \epsilon_{\rm RR})$ and $(\epsilon_{\rm LR}, \epsilon_{\rm RL})$ planes, there is an approximate "reflection symmetry" between $\epsilon_{\rm LL} \leftrightarrow \epsilon_{\rm RR}$ as well as between $\epsilon_{\rm LR} \leftrightarrow \epsilon_{\rm RL}$. As discussed in Sect. 2, the observables depend on $\sigma_{\rm LL} + \sigma_{\rm RR}$ and $\sigma_{\rm LR} + \sigma_{\rm RL}$, and to lowest order in the ϵ, this translates into a dependence on $\epsilon_{\rm LL} + \epsilon_{\rm RR}$ and $\epsilon_{\rm LR} + \epsilon_{\rm RL}$. Thus, in this approximation, the allowed regions would be bands at fixed $\epsilon_{\rm LL} + \epsilon_{\rm RR}$ and $\epsilon_{\rm LR} + \epsilon_{\rm RL}$, representing strong correlations between pairs of parameters. The contributions of the second-order effects (in the $\epsilon_{\alpha\beta}$) delimit and curve these bands. In the case of the $\epsilon_{\rm LR}$–$\epsilon_{\rm RL}$ exclusion region, the radius of curvature, given by an expression analogous to (16), is smaller than that of the $\epsilon_{\rm LL}$–$\epsilon_{\rm RR}$ exclusion region. This stronger bending originates from the destructive versus constructive interference between photon- and Z-exchange: above the Z resonance, $g^\ell_{\rm L} g^\ell_{\rm R} \chi_Z < 0$, whereas $(g^\ell_{\rm L})^2 \chi_Z \approx (g^\ell_{\rm R})^2 \chi_Z > 0$, so $|\mathcal{M}^{\rm SM}_{\rm LR}| = |\mathcal{M}^{\rm SM}_{\rm RL}| < |\mathcal{M}^{\rm SM}_{\rm LL}| \approx |\mathcal{M}^{\rm SM}_{\rm RR}|$.

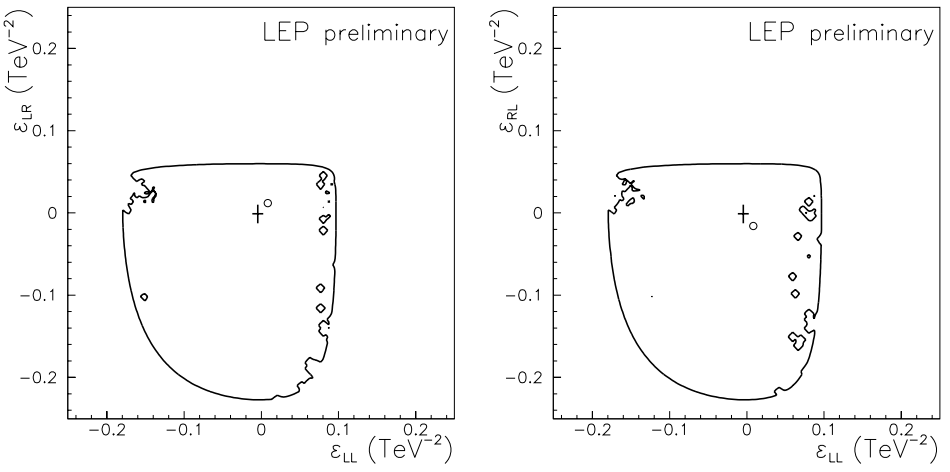

Fig. 2. The same as Fig. 1 for the $(\epsilon_{\rm LL}, \epsilon_{\rm LR})$ and $(\epsilon_{\rm LL}, \epsilon_{\rm RL})$ planes

In Fig. 2, we show the analogous allowed regions in the $(\epsilon_{\rm LL}, \epsilon_{\rm LR})$ and $(\epsilon_{\rm LL}, \epsilon_{\rm RL})$ planes. The allowed regions in the $(\epsilon_{\rm RR}, \epsilon_{\rm LR})$ and $(\epsilon_{\rm RR}, \epsilon_{\rm RL})$ planes are very similar to those of Fig. 2, and hence they are not shown.

In the figures, the constraints on the one-parameter models LL, RR LR and RL (see Table 2) are represented by bars. These correspond to one-dimensional model-dependent constraints at 95% C.L. with $\chi^2_{\rm CL} = 3.84$, obtained by varying only one parameter at a time with the remaining three set equal zero. The results in this case are in full agreement with those obtained in [3].

Figure 2 is rather different from Fig. 1, but the two panels are very similar among themselves. This is due to the symmetric inputs, $\sigma_{\rm LL} + \sigma_{\rm RR}$ and $\sigma_{\rm LR} + \sigma_{\rm RL}$, together with the fact that the linear approximation, determined by the interference between SM and CI couplings, provides a first, rough description of the bounds. Also, we note that there is little correlation between these pairs of parameters, and the allowed regions are simply

$$[\epsilon_{\alpha\beta} < \delta'] \cap [\epsilon_{\alpha'\beta'} < \delta'] \cap [\epsilon^2_{\alpha\beta} + \epsilon^2_{\alpha'\beta'} < \delta^2], \qquad (20)$$

where

$$\delta' \simeq \max(\epsilon_{\rm LL}) \quad \text{or} \quad \max(\epsilon_{\rm LR}) \quad \text{or} \quad \max(\epsilon_{\rm RL}), \qquad (21)$$

as determined from Fig. 1. Similarly,

$$\delta^2 = [\max(\epsilon_{\rm LL})]^2 + \{[\max(\epsilon_{\rm LR})]^2 \quad \text{or} \quad [\max(\epsilon_{\rm RL})]^2\}, \qquad (22)$$

respectively, for the two panels. This simple shape is thus due to the lack of correlations among the parameters shown in Fig. 2.

4 Discussion

Our most important result is that if one does not restrict the analysis to individual models, the bounds on the ϵ are rather loose. In fact, any set of three of them (but not all four, as is seen from the correlations in Fig. 1) can be of the order of $0.2\,{\rm TeV}^{-2}$. This corresponds to a scale $\Lambda \sim 2.2\,{\rm TeV}$.

In the case of $\epsilon_{\rm LL}$ and $\epsilon_{\rm RR}$, as discussed above, the orientation of the "banana" in Fig. 1 implies that $\epsilon_{\rm LL}$ and $\epsilon_{\rm RR}$ should roughly add to zero. Rather large deviations from the SM are allowed, *provided these parameters have opposite signs*. It should be noted that, if one assumes universality, such opposite signs can never arise from the low energy limit of a vector-particle exchange, irrespective of the chiralities of the couplings. This may in part explain why the present bounds are much looser than those of the model-dependent analyses.

Also, it should be stressed that we do not assume full lepton universality in this analysis. The muon and tau data are combined, but the couplings to those currents are not taken to be the same as the couplings to the electron of the initial state. If lepton universality were imposed, one would have the additional constraint $\epsilon_{\rm LR} = \epsilon_{\rm RL}$. Also, full lepton universality would imply the product $\epsilon_{\rm LL}\,\epsilon_{\rm RR} > 0$, and much of the allowed part of Fig. 1 would be excluded. We note that there are models without flavor universality, where $\epsilon_{\rm LL}$ and $\epsilon_{\rm RR}$ can have opposite signs (see, e.g. [17, 18]).

Up to this point, we have combined the muon and tau data. It is also interesting to study these two data sets separately. In Fig. 3 we show the contours which bound the allowed regions in the $(\epsilon_{\rm LL}, \epsilon_{\rm RR})$ and $(\epsilon_{\rm LR}, \epsilon_{\rm RL})$ planes for $e^+e^- \to \tau^+\tau^-$ (i.e., without using the muon data). The general shapes of these allowed regions are rather similar to those obtained from the combined data, but they are significantly larger. The corresponding allowed intervals of the ϵ parameters are given in Table 3, the analogue of Table 2. The model-independent global limits, for example, are looser than the combined muon and tau analysis by up to 40%. The muon data alone give shapes and allowed intervals quite similar to those in Fig. 3 and Table 3, respectively, but narrower, essentially reflecting the larger total error in the τ case.

In specific models, there are often constraints on these deviations $\epsilon_{\alpha\beta}$. For example, the Z' couplings of E_6 models lead to the constraints [19]:

$$Z'_\chi: \quad \epsilon_{\rm LR} = \epsilon_{\rm RL} < 0, \quad \epsilon_{\rm LL} = 9\,\epsilon_{\rm RR} < 0, \qquad (23)$$

$$Z'_\psi: \quad \epsilon_{\rm LR} = \epsilon_{\rm RL} > 0, \quad \epsilon_{\rm LL} = \epsilon_{\rm RR} < 0, \qquad (24)$$

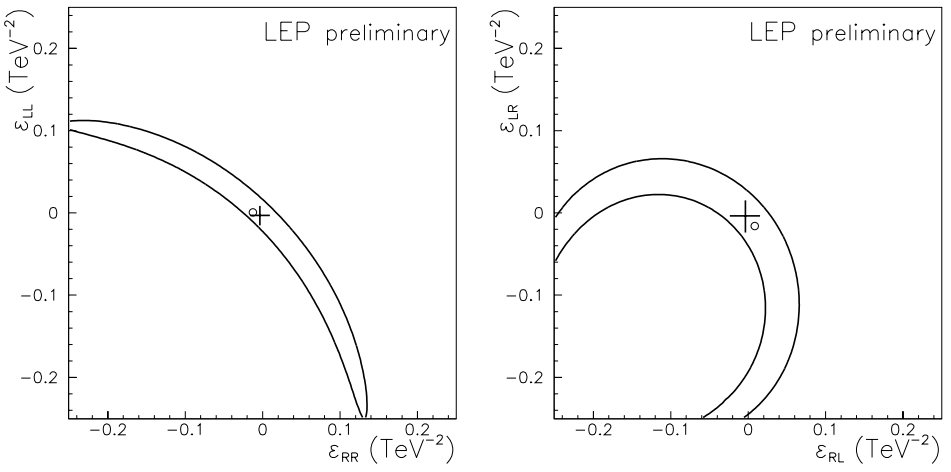

Fig. 3. Similar to Fig. 1, for tau data only

Table 3. Similar to Table 2, for final-state τ pairs only

Parameter	Model independent		Model dependent
(TeV^{-2})	central value	global limits	
$\epsilon_{\rm LL}$	0.0005	$(-0.249, 0.113)$	$-0.0032^{+0.0118}_{-0.0120}$
$\epsilon_{\rm RR}$	-0.0125	$(-0.258, 0.136)$	$-0.0035^{+0.0129}_{-0.0131}$
$\epsilon_{\rm LR}$	-0.016	$(-0.273, 0.066)$	$-0.0036^{+0.0188}_{-0.0202}$
$\epsilon_{\rm RL}$	0.0085	$(-0.273, 0.066)$	$-0.0036^{+0.0188}_{-0.0202}$

$$Z'_\eta: \quad \epsilon_{\rm LR} = \epsilon_{\rm RL} < 0, \quad \epsilon_{\rm LL} = \frac{1}{4}\,\epsilon_{\rm RR} < 0. \qquad (25)$$

These signs are given by the signs of the couplings, together with the low energy limit of the propagator. The leptonic data studied here lead to the $M_{Z'}$ bounds: Z'_χ: 600 GeV; Z'_ψ: 330 GeV; Z'_η: 340 GeV. The corresponding bounds from all data [3] are 670 GeV, 480 GeV and 430 GeV, respectively.

Also, in the case of models with TeV-scale extra dimensions (with Kaluza–Klein excitations of the photon and the Z), there are relations among the couplings [20]: $\epsilon_{\rm LR} = \epsilon_{\rm RL} < 0$, and $\epsilon_{\rm LL} = \epsilon_{\rm RR}/4s^2_{\rm W} \simeq \epsilon_{\rm RR} < 0$. For one extra dimension, the bound on the compactification scale [21] is $M_c > 2.2$ TeV.

As anticipated in the Introduction, we shall here consider an example application, namely the effects of anomalous gauge couplings [17] in the process (1). We note that this model, which assumes universality, is characterized by two parameters, f_{DB} and f_{DW}. The deviations (7) will take the form

$$\epsilon_{\rm LL} = \alpha_{\rm e.m.}\left(\frac{\tilde f_{DW}}{2s^2_{\rm W}} + \frac{2\tilde f_{DB}}{c^2_{\rm W}}\right), \quad \epsilon_{\rm RR} = \alpha_{\rm e.m.}\frac{8\tilde f_{DB}}{c^2_{\rm W}},$$
$$\epsilon_{\rm LR} = \epsilon_{\rm RL} = \alpha_{\rm e.m.}\frac{4\tilde f_{DB}}{c^2_{\rm W}}, \qquad (26)$$

where $\tilde f_{DB}$ and $\tilde f_{DW}$ are related to f_{DB} and f_{DW} of [17] by $\tilde f = f/m_t^2$. In this model, one has $\epsilon_{\rm LR} = \epsilon_{\rm RL}$, so any deviation would be restricted to lie along the dashed line in Fig. 4, which shows a magnification of the allowed band in Fig. 1 (right panel) for $\chi^2_{\rm CL} = 5.99$, corresponding to two parameters. The intersections with the allowed bounds allow us to set a limit on $|\tilde f_{DB}| < 0.21\,{\rm TeV}^{-2}$. This also amounts to a bound on $\epsilon_{\rm RR}$. From the analogue of Fig. 1 (left panel), corresponding to two parameters, one can extract bounds on $\epsilon_{\rm LL}$. Using (26), these can then be converted to the bounds: $-1.7\,{\rm TeV}^{-2} < \tilde f_{DW} < 1.1\,{\rm TeV}^{-2}$.

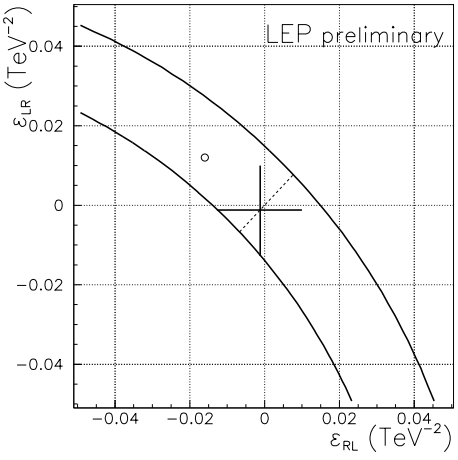

Fig. 4. Similar to Fig. 1 (right panel), but magnification of the region of small $\epsilon_{\rm LR}$ and $\epsilon_{\rm RL}$, for $\chi^2_{\rm CL} = 5.99$. The diagonal line corresponds to the constraint of the anomalous gauge coupling model

We have not analyzed the quark data, which are of poorer quality, due to the limited efficiency of b-tagging, together with the problem of distinguishing b from $\bar b$ jets (see, however, [22]).

At the Linear Collider, where polarization would be available, more observables can be studied, such as $A_{\rm LR}$ and $A_{\rm LR,FB}$. Thus, and because of the higher energy, dramatically tighter constraints are foreseen [9].

Acknowledgements. This research has been supported by the Research Council of Norway, by MIUR (Italian Ministry of University and Research) and by funds of the University of Trieste. We would like to thank our colleagues of the Alice,

BaBar and Compass collaborations for the use of their computing facilities, which significantly sped up our work.

References

1. G. 't Hooft, in Recent Developments In Gauge Theories, Proceedings, Nato Advanced Study Institute, Cargese, France, August 26–September 8, 1979, edited by G. 't Hooft, C. Itzykson, A. Jaffe, H. Lehmann, P.K. Mitter, I.M. Singer, R. Stora (Plenum, New York 1980) (Nato Advanced Study Institutes Series: Series B, Physics, 59); S. Dimopoulos, S. Raby, L. Susskind, Nucl. Phys. B **173**, 208 (1980)
2. E. Eichten, K.D. Lane, M.E. Peskin, Phys. Rev. Lett. **50**, 811 (1983); R. Ruckl, Phys. Lett. B **129**, 363 (1983)
3. LEPEWWG $f\bar{f}$ SubGroup (C. Geweniger et al.), Combination of the LEP II e^+e^- Results, CERN preprint LEP2FF/02-01 (March 2002); ALEPH Collaboration and DELPHI Collaboration and L3 Collaboration and OPAL Collaboration and LEP Electroweak Working Group and SLD Heavy Flavor and Electroweak Groups (D. Abbaneo et al.), A combination of preliminary electroweak measurements and constraints on the standard model, CERN-EP-2001-098, LEPEWWG-2001-02 [hep-ex/0112021]
4. V.D. Barger, K. m. Cheung, K. Hagiwara, D. Zeppenfeld, Phys. Rev. D **57**, 391 (1998) [hep-ph/9707412]; D. Zeppenfeld, K. m. Cheung, Proceedings of 5th International WEIN Symposium: A Conference on Physics Beyond the Standard Model (WEIN 98), Santa Fe, NM, 14–21 Jun 1998; preprint MADPH-98-1081 [hep-ph/9810277]
5. G. Altarelli, J.R. Ellis, G.F. Giudice, S. Lola, M.L. Mangano, Nucl. Phys. B **506**, 3 (1997) [hep-ph/9703276]; R. Casalbuoni, S. De Curtis, D. Dominici, R. Gatto, Phys. Lett. B **460**, 135 (1999) [hep-ph/9905568]; V.D. Barger, K. m. Cheung, Phys. Lett. B **480**, 149 (2000) [hep-ph/0002259]
6. H. Kroha, Phys. Rev. D **46**, 58 (1992)
7. J.A. Aguilar-Saavedra et al. [ECFA/DESY LC Physics Working Group Collaboration], TESLA Technical Design Report Part III: Physics at an e^+e^- Linear Collider, [hep-ph/0106315]; T. Abe et al. [American Linear Collider Working Group Collaboration], Linear collider physics resource book for Snowmass 2001. 1: Introduction, in Proceedings of the APS/DPF/DPB Summer Study on the Future of Particle Physics (Snowmass 2001) edited by N. Graf [hep-ex/0106055]
8. A.A. Babich, P. Osland, A.A. Pankov, N. Paver, Phys. Lett. B **476**, 95 (2000) [hep-ph/9910403]
9. A.A. Babich, P. Osland, A.A. Pankov, N. Paver, Phys. Lett. B **518**, 128 (2001) [hep-ph/0107159]
10. A.A. Pankov, N. Paver, Phys. Lett. B **493**, 307 (2000) [hep-ph/0009117]
11. B. Schrempp, F. Schrempp, N. Wermes, D. Zeppenfeld, Nucl. Phys. B **296**, 1 (1988)
12. M. Consoli, W. Hollik, F. Jegerlehner, in Z Physics at LEP1, edited by G. Altarelli, R. Kleiss, C. Verzegnassi, vol. 1, p. 7, 1989
13. G. Altarelli, R. Casalbuoni, D. Dominici, F. Feruglio, R. Gatto, Nucl. Phys. B **342**, 15 (1990)
14. D.Y. Bardin, P. Christova, M. Jack, L. Kalinovskaya, A. Olchevski, S. Riemann, T. Riemann, Comput. Phys. Commun. **133**, 229 (2001) [hep-ph/9908433]
15. F. James, M. Roos, Comput. Phys. Commun. **10**, 343 (1975)
16. K. Hagiwara et al. [Particle Data Group Collaboration], Phys. Rev. D **66**, 010001 (2002)
17. G.J. Gounaris, D.T. Papadamou, F.M. Renard, Phys. Rev. D **56**, 3970 (1997) [hep-ph/9703281]
18. K.R. Lynch, S. Mrenna, M. Narain, E.H. Simmons, Phys. Rev. D **63**, 035006 (2001) [hep-ph/0007286]
19. A. Leike, Phys. Rept. **317**, 143 (1999) [hep-ph/9805494]; K. m. Cheung, Phys. Lett. B **517**, 167 (2001) [hep-ph/0106251]
20. G. Pasztor, M. Perelstein, in Proceedings of the APS/DPF/DPB Summer Study on the Future of Particle Physics (Snowmass 2001) edited by N. Graf, hep-ph/0111471
21. T.G. Rizzo, J.D. Wells, Phys. Rev. D **61**, 016007 (2000) [hep-ph/9906234]
22. Y. Inoue et al. [TOPAZ Collaboration], Eur. Phys. J. C **18**, 273 (2000) [hep-ex/0012033]